A Novel Multifaceted Virtual Craniofacial Surgery Scheme Using Computer Vision

A.S. Chowdhury[1,*], S.M. Bhandarkar[1], E.W. Tollner[2], G. Zhang[2], J.C. Yu[3], and E. Ritter[3]

[1] Department of Computer Science,
The University of Georgia, Athens GA 30602 -7404, USA
{ananda, suchi}@cs.uga.edu
[2] Dept. of Biological & Agricultural Engg,
The University of Georgia, Athens, GA 30602 – 4435, USA
{btollner, gzhang}@engr.uga.edu
[3] Dept. of Plastic Surgery,The Medical College of Georgia,
Augusta, GA 30912, USA
{jyu, eritter}@mcg.edu

Abstract. The paper addresses the problem of virtual craniofacial reconstruction from a set of Computer Tomography (CT) images, with the multiple objectives of achieving accurate local matching of the opposable fracture surfaces and preservation of the global shape symmetry and the biomechanical stability of the reconstructed mandible. The first phase of the reconstruction, with the mean squared error as the performance metric, achieves the best possible local surface matching using the Iterative Closest Point (ICP) algorithm and the Data Aligned Rigidity Constrained Exhaustive Search (DARCES) algorithm each used individually and then in a synergistic combination. The second phase, which consists of an angular perturbation scheme, optimizes a composite reconstruction metric. The composite reconstruction metric is a linear combination of the mean squared error, a global shape symmetry term and the surface area which is shown to be a measure of biomechanical stability. Experimental results, including a thorough validation scheme on simulated fractures in phantoms of the craniofacial skeleton, are presented.

1 Motivation

In modern society, craniofacial fractures are encountered very frequently with the two most prominent causes being gunshot wounds and motor vehicle accidents [1]. These frequently encountered fractures possess some distinct patterns. Sometimes, the patterns imply a single fracture, and, in some other cases, there can be a combination of single fractures [2]. From the surgical standpoint, fractures are fixated one at a time in the operating room and thus can and must be so decomposed in the pre-surgical planning as well. Thus, practically speaking, in almost all the cases, reconstruction

* Corresponding author's e-mail: ananda@cs.uga.edu

Y. Liu, T. Jiang, and C. Zhang (Eds.): CVIBA 2005, LNCS 3765, pp. 146 – 159, 2005.

from a single mandibular fracture assumes paramount importance. The plastic surgeon in the operating room restores the form and function of the fractured bone elements in the craniofacial skeleton typically by first exposing all the fragments, then returning them to their normal configuration, and finally maintaining these reduced bone pieces with rigid screws and plates. However, there are several critical and inherent limitations to this current, standard approach. To visualize the fragments in order to reduce them necessitates their exposure which consequently reduces the attached blood supply. To improve the blood supply, one can decrease the extent of dissection. However this means not being able to visualize the entire fracture, which could lead to potential misalignments of the bone fragments. Additionally, the cost of surgery becomes prohibitive with the increased operating time necessary to ensure an accurate reconstruction, especially in complex cases [3]. An elaborate virtual reconstruction scheme involving a single mandibular fracture is proposed in this work which can potentially reduce the operating time and consequently, the cost of surgery without sacrificing surgical precision, thus drastically reducing the operative and post-operative patient trauma.

2 Literature Review and Our Contribution

A lot of interesting research has been performed over the past decade in various aspects of craniofacial/maxillofacial surgery. Because of space limitations, only a few representative works are mentioned here. The mass tensor model is used for fast soft tissue prediction in [4] whereas the mass-spring model is used for fast surgical simulation from CT data in [5]. The problem of building a virtual craniofacial patient from CT data has been addressed in [6] whereas a reconstruction approach involving complete 3D modeling of the solid high-detailed structure of the craniofacial skeleton, starting from the information present in the 3D diagnostic CT images can be found in [7]. The *Iterative Closest Point (ICP)* [8] algorithm is seen to be a popular computer vision algorithm for surface registration in the field of medical imaging. Some variants of the ICP algorithm that incorporate certain statistical concepts such as Expectation Maximization (EM) in the context of medical imaging can be found in [9]. The basic benefit of the ICP algorithm is that it gives an accurate result given a good initial starting point. Another surface registration algorithm called the *Data Aligned Rigidity Constrained Exhaustive Search (DARCES)* which incorporates a *Random Sample Consensus (RANSAC)* model fitting approach [10], is popular because of its robustness to outliers and has also been used in medical imaging [11].

In this paper, we address the problem of single fracture craniofacial reconstruction from broken solid fragments. Our principal contribution is the formulation of a novel two-phase virtual reconstruction scheme. The first phase of our proposed reconstruction scheme employs the *ICP* and *DARCES* algorithms first individually and then in a novel synergistic combination. The ICP algorithm in our implementation solves the 3D correspondence problem using Bipartite Graph Matching. The synergetic combination of the two algorithms, where the output of the DARCES algorithm is fed as an input to the ICP algorithm, is observed to result in an improved

surface matching algorithm with a considerable reduction in both, the mean squared error (MSE) and the execution time. We briefly describe the first phase of reconstruction in this paper and refer the interested reader to our previous work in [12]. The anatomy of the human mandible clearly exhibits bilateral symmetry. Furthermore, basic biophysical principles indicate that the most stable state for a solid body is the state with minimum energy [13] and this fact should be applicable to the human mandible as well. Since both the ICP and DARCES algorithms are essentially data driven and are purely local in nature, the first phase cannot explicitly guarantee the preservation of either the global shape symmetry or the biomechanical stability of the reconstructed human mandible. The incorporation of anatomical shape knowledge in medical image registration has been discussed in [14, 15]. However, we go one step further in the second phase of our reconstruction paradigm. In the second phase, a composite reconstruction metric is introduced and expressed as a linear combination of three different terms, namely (a) the MSE, (b) a global shape symmetry term and (c) a surface area term (which is shown to be a measure of biomechanical stability). An angular perturbation scheme is used to optimize the composite reconstruction metric. Thus the second reconstruction phase enables us to explore and address, in an innovative manner, the anatomical shape preservation as well as biophysical stability issues in the reconstruction paradigm (which may not be always possible in the operating room). As shown in this paper, the second phase of reconstruction integrates computer vision algorithms with ideas from biophysics and mathematics to generate a more accurate reconstruction.

3 Image Preprocessing

The input to the system (Fig.1) is a sequence of 2D grayscale images of a fractured human mandible, generated via Computer Tomography (CT). Each image slice is 150 mm x 150 mm with an 8-bit color depth. A simple thresholding scheme is used to binarize each CT image slice (Fig. 2b). A 2D Connected Component Labeling (CCL) algorithm in conjunction with an area filter is used to remove some unwanted artifacts (Fig. 2c). The results of the 2D CCL algorithm are propagated across the CT image slices, resulting in a 3D CCL algorithm. Interactive contour detection is then performed on all the 2D CT slices. The contour points from the CT image stack are assembled to form a 3D surface point data set. The data sets resulting from two opposable fracture surfaces are denoted as the sample dataset and the model dataset.

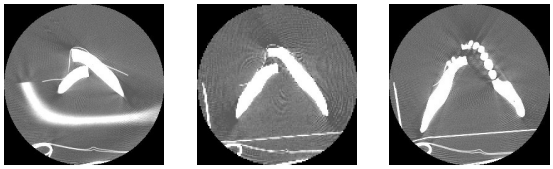

Fig. 1. A sequence of CT images (where higher intensity values represent mandible fragments and artifacts and lower intensity values represent soft tissue)

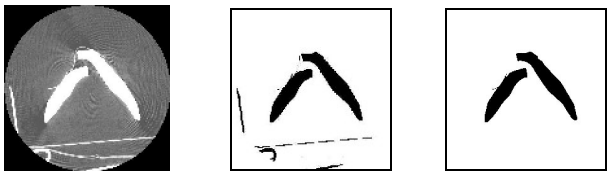

Fig. 2. (a) A typical 2D CT slice. (b) The CT slice after thresholding. (c) The CT slice after Connected Component Labeling and Size Filtering. In (b) and (c), the lower intensity values represent mandible fragments and artifacts.

4 Reconstruction Phase I - Surface Matching Algorithms

The first phase of the virtual reconstruction consists of applications of the ICP, DARCES and hybrid DARCES-ICP algorithms. For the ICP algorithm [8], the matching point pairs (forming the *closest set*) are determined in a novel fashion using the Maximum Cardinality Minimum Weight (MCMW) Bipartite Graph Matching algorithm [16] based on the Hungarian Marriage method proposed by Kuhn [17]. The 3D sample and model data sets correspond to the two disjoint vertex sets (V_1, V_2) in a bipartite graph $G(V, E)$. The edge-weight $(W_{ij} \in E)$ between any two nodes i and j (such that $i \in V_1$ and $j \in V_2$) is deemed to be the Euclidean distance between them. Note that the Euclidean distance is invariant to a 3D rigid body transformation. The bipartite graph matching implicitly preserves the local shape of the two surfaces (to be registered) with arbitrary orientation, without necessitating their pre-alignment. The edge weights are given by:

$$W_{ij} = ((x_i - x_j)^2 + (y_i - y_j)^2 + (z_i - z_j)^2)^{1/2} \tag{1}$$

The MSE (ξ^2) is given by:

$$\xi^2 = (1/N)\sum_{i=1}^{N} \left\| c_i - (Rs_i + T) \right\|^2 \tag{2}$$

where R denotes the rotation matrix, T, the translation vector, s_i, a point in the sample data set and c_i, the corresponding point in the closest set. A pre-specified error convergence criterion of 0.001 was used. A RANSAC-based approach for the DARCES algorithm was adopted [10]. All the 3D rigid body transformation parameters were computed using the Singular Value Decomposition (SVD) algorithm [18]. A novel synergistic combination of the DARCES and ICP algorithms, where the inputs to the ICP algorithm are the original model set and, the sample set transformed by the DARCES algorithm, was employed [12]. The ICP algorithm yields an accurate 3D rigid body transformation but is sensitive to outliers in the input data. The DARCES algorithm, on the other hand, enables outlier rejection but the computed transformation is only approximate. In the DARCES-ICP hybrid algorithm, the pairs of matched points generated by the DARCES algorithm serve to reduce the cardinalities of the two data sets to be matched (using bipartite graph matching) in the ICP algorithm. Consequently, the dense bipartite graph used to determine the *closest*

set in the ICP algorithm is reduced to a sparse bipartite graph with fewer nodes and edges. Thus, the subsequent MCMW bipartite graph matching procedure in the ICP algorithm has a lower execution time since it is run on a more meaningful (in terms of the number of pairs of matching points in the two vertex sets V_1 and V_2) sparse bipartite graph. Also, a much lower MSE is achieved by the ICP algorithm for the matching of the two fracture surfaces, since the DARCES algorithm provides a better starting point to the ICP algorithm by virtue of outlier removal. We have also achieved further improvement in local surface matching with suitable modeling of surface irregularities and their incorporation in the reconstruction scheme [19].

5 Identification of the Plane of Bilateral Symmetry

In order to ensure preservation of the global shape of the reconstructed human mandible, the plane of bilateral symmetry [20] – [24] is determined for the reconstructed human mandible. We assume the general equation of a three-dimensional plane to be:

$$F(x, y, z) = Ax + By + Cz - D = 0 \tag{3}$$

It is well known that the planes of reflection symmetry for any rigid body pass through its centre of mass and that their coefficients are the components of the eigenvectors of the real symmetric moment of inertia matrix/tensor [13]. This fact allows us to determine the possible candidates for the planes of reflection symmetry without recourse to exhaustive search [23]. The elements of the 3x3 moment of inertia matrix/tensor are the second order centralized moments for the rigid body under consideration. Once the coefficients of the three symmetry planes are determined, the entire mandible is reflected about each of these planes. For each point *f(x, y, z)* in the reconstructed mandible, there exists a corresponding point $f_R(x, y, z)$ in the reflected mandible, given by the following equation [21]:

$$f_R(x,y,z) = \begin{cases} f(x,y,z) - 2\dfrac{F(f)}{\|\nabla F\|}\dfrac{\nabla F}{\|\nabla F\|} \; if\; F(f) > 0 \\ f(x,y,z) + 2\dfrac{F(f)}{\|\nabla F\|}\dfrac{\nabla F}{\|\nabla F\|} \; otherwise \end{cases} \tag{4}$$

where the F is computed using equation (3). There are various measures of symmetry to be found in the literature such as the sum of absolute distance and the normalized cross- correlation [20 - 23]. The proposed metric is a linear combination of the normalized cross-correlation and a novel set-theoretic measure. If one treats the reconstructed mandible g and the reflected mandible h as two N-dimensional vectors, the normalized cross-correlation γ between g and h is given by [20, 21, 24]:

$$\gamma(g,h) = \frac{(g - \bar{g}u).(h - \bar{h}u)}{\left\|g - \bar{g}u\right\| \quad \left\|h - \bar{h}u\right\|} \tag{5}$$

where $\bar{g}$ and $\bar{h}$ are the means of the elements of g and h respectively and u is an N-dimensional unit vector. Alternatively, g and h can be considered as two 3D data sets of cardinality n. A novel set theoretic term β is introduced as a measure of overlap between the sets g and h:

$$\beta = 1 - \frac{|g \quad \Delta \quad h|}{|g \quad \cup \quad h|} \tag{6}$$

where Δ denotes the symmetric difference between and $\cup$ represents the union of the reconstructed mandible set g and the reflected mandible set h. Interestingly, β lies between 0 (when there is no overlap between g and h) and 1 (when there is perfect overlap between g and h). The proposed metric for global shape symmetry, denoted by GM, is given by:

$$GM = \lambda_1 * \gamma + \lambda_2 * \beta \tag{7}$$

$$\text{where } \sum_{i=1}^{2} \lambda_i = 1 \tag{8}$$

Depending on the problem structure and image representation, different values of λ_1 and λ_2 can be chosen. We assume $\lambda_1 = \lambda_2 = 0.5$ for our present problem. The plane with the largest value of GM is deemed to be the plane of bilateral symmetry.

6 Estimation of Biomechanical Stability

Surface energy minimization is modeled along the well accepted principle of strain potential minimization, which, in turn, is based on minimization of the strain energy of an isotropic solid. The strain potential (U) can be defined as follows:

$$U = \iiint_V f(\text{normal and shear strains, Young's and shear moduli, Poisson ratio})\, dv \tag{9}$$

Details of the functional form of f for an isotropic solid may be found in [25]. The normal and shear strains occurring in response to a force field are represented by a displacement field u and resisted by forces arising from the Young's and shear moduli. A body force B (operating on a volume V with surface area S) and surface shear forces T will result in a deformation pattern that minimizes U. Further, it can be shown that the following criterion must be satisfied under equilibrium conditions [25]:

$$\iint_S T.\delta u \delta a + \iiint_V B.\delta u \delta v - \delta U = 0 \tag{10}$$

The integral on the left in equation (10) is a surface energy term. For the purpose of this discussion, we may assume near zero resistance to movement resulting from a force of unity, thus the energy related to volumetric response is near zero. Hence it can be concluded that a minimum potential energy state results in minimum surface energy. Further, minimum surface energy in the context of moving fragments with

constant surface force is consistent with minimum surface area. So, a biomechanically stable state (i.e. a state with minimum potential energy) is guaranteed by a state with minimum surface area. Only the top and bottom curved surfaces (of the six possible surfaces) of the human mandible in the CT image stack, that account for the maximum contribution to the total surface area, are considered. Each surface (S) can be modeled of as an aggregation of disjoint surface patches (SP) [26]:

$$S = \bigcup_{i=1}^{n} SP_i \tag{11}$$

$$SP_i \cap SP_j = \phi \quad if \quad i \neq j \tag{12}$$

The determinant (gm) of the first fundamental form matrix **G** [26, 27] for each surface patch is computed using techniques of differential geometry. The area of each surface (SA), in terms of its constituent surface patch areas (SPA) and metric determinants (gm), is given by the following equation:

$$SA = \sum_{i=1}^{n} gm_i^{1/2} * SPA_i \tag{13}$$

where n is the number of surface patches comprising a given surface. Each digital surface (patch) is approximated by an analytic surface (patch) using a least-squares surface fitting technique [26, 27]. Discrete bi-orthogonal Chebyshev polynomials are used as the basis functions for each such surface patch within an N x N window (where $N = 5$ in our case). The surface function estimate that minimizes the sum of squared surface fitting error within the window is given by:

$$\hat{f}(u,v) = \sum_{i,j=0}^{3} a_{i,j} \varphi_i(u) \varphi_j(v) \tag{14}$$

where the φ_i's are the basis functions for the Chebyshev polynomials. Coefficients of the functional approximation are given by:

$$a_{i,j} = \sum_{(u,v)=(-M,-M)}^{(u,v)=(M,M)} f(u,v) b_i(u) b_j(v) \tag{15}$$

where $M= (N-1)/2$ and the b_i's are the normalized versions of the above polynomials. From the estimated coefficients, the first and second order partial derivatives of the fitted surface patch are computed. These partial derivatives are used to compute the elements of the first fundamental form matrix **G** of the fitted surface patch. Finally, the determinant gm of the matrix **G** for that surface patch is computed [26, 27].

7 Reconstruction Phase II - Angular Perturbation Scheme

The rationale behind the second phase of the reconstruction scheme, which consists of an angular perturbation scheme, is to arrive at a reconstruction that minimizes the

MSE between the matched fracture surfaces and also yields the best possible shape symmetry and biomechanically, the most stable configuration. A normalized composite reconstruction metric (*CRM*), which is a linear combination of the MSE, the inverse of the global shape symmetry (since the optimization problem is formulated as one of minimization) and the surface area (as a measure of surface energy, which, in turn, determines biomechanical stability) is proposed as a performance measure for the perturbation scheme and is given by:

$$CRM = \alpha_1 * \xi^2 + \alpha_2 * GM^{-1} + \alpha_3 * ((TSA + BSA)/2) \tag{16}$$

where ξ^2 is the MSE, *GM* is given by equation (7), and *TSA* and *BSA* denote the top and bottom surface areas respectively and are estimated using equation (13). The α_i 's are determined using the following equation:

$$\frac{\alpha_1}{\left|\partial(\xi^2)\right|} = \frac{\alpha_2}{\left|\partial(GM^{-1})\right|} = \frac{\alpha_3}{\left|\partial((TSA + BSA)/2)\right|};\ \sum_{i=1}^{3} \alpha_i = 1 \tag{17}$$

where $\left|\partial(t)\right|$ denotes the normalized absolute difference (i.e. difference of the maximum and minimum values, divided by the maximum value) of the term *t* over the range of perturbation. One of the rationales behind model generation is to exploit certain key anatomical measurements to fine tune the coefficients in the equation (16). However, presently, these coefficients are computed based on the normalized absolute differences of the associated factors over the range of angular perturbations (see Fig. 5). The perturbations are applied to the fracture site in steps of 0.2^0 from -1^0 to $+1^0$ about each of the x, y and z axes. In each perturbed state, a new *CRM* is estimated after re-computing all the three components in equation (16). The small range of angular perturbations is justified based on a reasonable expectation that the locally best (minimum MSE yielding) solution generated by the DARCES-ICP hybrid algorithm is not very far off from the best overall solution (resulting the minimum *CRM* value). The choice of angular quantization (0.2^0) is a judicious compromise between execution time and accuracy. The smaller the angular quantization, higher the execution time of the algorithm. On the contrary, making the angular quantization too large may prevent the algorithm from arriving at the best possible solution. The state generating the minimum *CRM* value is deemed to be the desired reconstruction.

8 Experimental Results and Analysis

The reconstructed images for the DARCES, ICP and hybrid DARCES-ICP algorithms are presented in Fig. 3. In Fig. 4, the projections, along each of the coordinate axes, of the 3D reconstruction obtained using the hybrid DARCES-ICP algorithm are visually compared with the projections of the original mandible.

The quantitative reconstruction results (i.e., the MSE), obtained by using the various surface matching algorithms (described in Section 4) are shown in Table 1. Table 2 shows typical values for the parameters γ, β and *GM* (in the equations (5), (6)

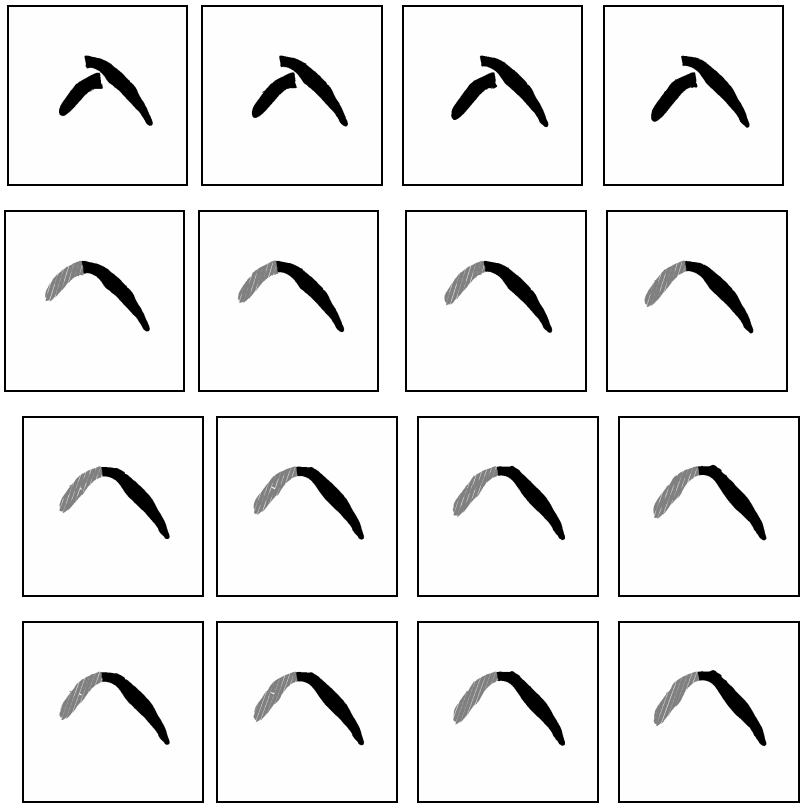

Fig. 3. The first row represents broken mandible fragments in typical CT slices. The second, third and fourth rows respectively represent reconstruction resulting from ICP, DARCES and hybrid DARCES-ICP algorithms.

and (7) respectively) for the three different candidate symmetry planes in the unperturbed state. The variations of the mean squared error, the inverse global metric for the plane of the bilateral symmetry, the average surface area and the normalized composite reconstruction metric as a function of angular perturbations along all the three major axes are graphically portrayed in Figs. 5(a)-5(d) respectively. The ranges of variations for these parameters along with their coefficients in equation (17) are shown in Table 3. Interestingly, with the incorporation of very small angular perturbations, it is possible to attain a reconstruction state, which not only yields better results in terms of the average surface area and shape symmetry, but also significantly reduces the local MSE. This is clearly revealed in Table 4, where the first and the second row respectively show the values of different terms of equation (16) for the unperturbed configuration (i.e. the reconstruction generated by the hybrid DARCES-ICP algorithm) and the optimal configuration (for a perturbation of -0.4^0 about the x-axis, yielding the minimum normalized *CRM* value). These results show the effectiveness of the novel second phase of the proposed virtual reconstruction.

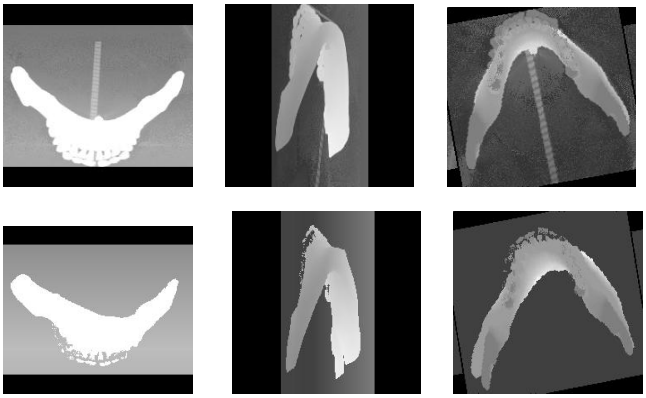

Fig. 4. Comparison of the original and reconstructed mandibles. The top row is the original mandible and the bottom row is the reconstructed mandible obtained using DARCES-ICP hybrid algorithm. The first, second and the third columns represent the 3D projections along the x, y and z axes respectively.

Table 1. A comparison of MSE values obtained by applying various surface matching algorithms [12, 19]

Surface Matching Scheme	MSE (mm^2)
ICP	0.91
DARCES	0.33
Hybrid DARCES-ICP	0.25

Table 2. Symmetry plane determination for a typical unperturbed state resulting from phase-I of the reconstruction

γ	β	*GM*	Equation of the Plane	Comment
0.79	0.88	0.83	0.98x – 0.16y + 0.12z = 65.42	Plane of Bilateral Symmetry
0.27	0.72	0.50	-0.20x + 0.87y – 0.45 z = 58.78	-
0.35	0.82	0.59	-0.03x + 0.47y + 0.88z = 50.95	-

Table 3. Comparison of the normalized variations of the different terms in eqn. (16) and their coefficients in eqn. (17)

	MSE	Inverse Global Symmetry	Average Surface Area
Variations	0.86	0.07	0.12
Coefficients	0.82	0.06	0.11

The experimental results and subsequent analysis presented in this section are for a typical single fracture reconstruction which is carried out using our developed software *InSilicoSurgeon* [12], which is built on top of *ImageJ*, the imaging software from *NIH* [28]. Our software contains a simple but elegant Graphical User Interface

Table 4. Comparison of the performance measures associated with the optimal state (-0.4^0 rotation about x-axis) and the unperturbed state (the MSE, Inverse_GM, Average Surface Area and CRM values are all normalized).

Axis	Angle	MSE	Inverse_GM	Average Surface Area	*CRM*
x	-0.4^0	0.138	0.952	0.892	0.275
-	-	0.148	0.964	0.982	0.293

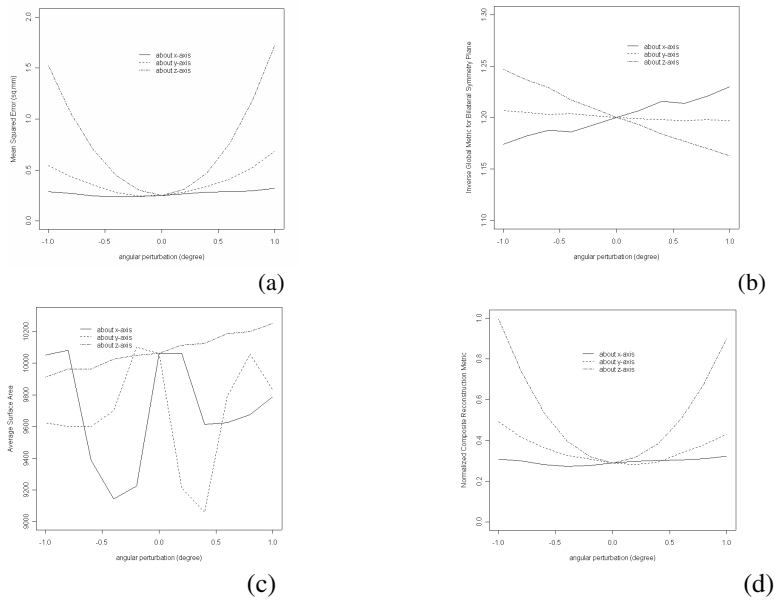

Fig. 5. Variations in the (a) mean squared error (ξ^2) (b) Inverse Global Metric for the Plane of Bilateral Symmetry (GM^{-1}) (c) Average Surface Area ((TSA + BSA/2)) (d) Normalized *CRM*, with angular perturbation along all the three major axes

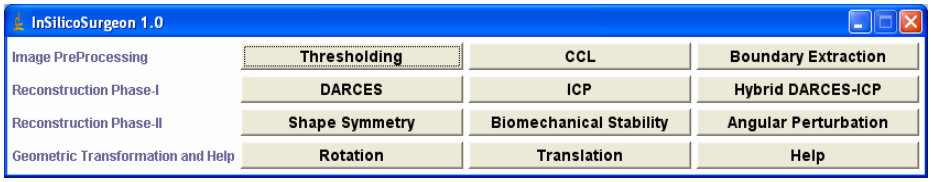

Fig. 6. A snapshot of the developed GUI where the extreme left column describes various stages of the reconstruction and each button performs a dedicated task (is evident from the name of the button)

(GUI) which can be of substantial help for virtual surgery as well as surgical training purposes. A *Help* button is provided for general guidance. The *Geometric Transformation* button (see Fig. 6) is used to finally bring the various bone fragments into registration.

9 Model Generation and Validation of the Virtual Reconstruction

In addition to the visual comparison and qualitative estimation of the accuracy of the virtual craniofacial reconstruction, we used solid modeling for further validation. The serial images of the reconstructed human mandible were loaded into the 3D Doctor software [29] which builds the virtual solid model from the serial CT scans and facilitates initial processing and 3-D viewing. Solid models were saved in the STL file format for prototype development and further analyses. The solid models were printed on a StratoSys rapid prototype printer (model: Dimension, software: Catalyst 3.4)[1], which reproduces a solid model by layering high density polyethylene plastic in 4 nm layers with repeated passes. A comparison of key anatomical measurements between the reference and reconstructed mandible were made. The STL files were transformed via AutoCAD into a Pro/E compatible file format for Finite Element (FE) analyses. Research is also currently underway for assigning appropriate material properties and for identifying a suitable constitutive model for the mandible material.

10 Conclusions and Future Work

The paper addressed the important problem of virtual craniofacial reconstruction with multiple objectives of obtaining accurate local surface matching as well as ensuring global shape preservation and biomechanical stability of the reconstructed human mandible. The present application can be used as a pre-surgical planning tool and as a training tool for surgical residents. In phase-I of the reconstruction, two different classes of algorithms namely the ICP and the DARCES were first applied individually and then in a cascaded manner for accurate surface matching. The combination of the two algorithms resulted in an improved MSE, and a considerable reduction in the execution time compared to the ICP algorithm used in isolation. The plane of bilateral symmetry was computed for the best possible reconstruction resulting from the first phase, using a novel combination of the normalized cross-correlation and a set theoretic measure. Minimization of surface area was shown to be mathematically equivalent to minimization of surface energy and used as a measure of biomechanical stability. The average surface area was estimated for the best reconstructed mandible resulting from the first phase. A composite reconstruction metric, expressed as a linear combination of the mean squared error, global shape symmetry and surface area, was introduced as a performance measure in the second phase of the reconstruction. A local search in this phase, based on an angular perturbation scheme, was shown to result in a solution that minimizes the composite reconstruction metric instead of just the MSE alone. A validation scheme was proposed to measure the effectiveness of the entire reconstruction by generation of a solid model of the reconstructed mandible. It is important to note that although the experiments thus far have been performed on phantom data sets (experiments on real data sets are ongoing), our reconstruction paradigm, with the statistically robust RANSAC-based DARCES algorithm, as an integral component, is adequate to handle the issue of outliers and missing data in case of real data sets. The hybrid DARCES-ICP algorithm could be expected to provide an accurate reconstruction (with lower MSE) followed by the

[1] 14950, Martin Dr. Eden Prairie, MN 55344, USA.

second reconstruction phase to guarantee a minimum *CRM* value on real data sets. Future research will involve (i) model guided feedback to fine tune the coefficients of the different terms in the composite metric in equations (16) and (17) to result in an even better reconstruction, and (ii) extending the present single fracture reconstruction framework to multiple fractures using a combinatorial optimization approach.

References

1. R. E. King, J.M. Scianna and G.J. Petruzzelli, Mandible fracture patterns: a suburban trauma center experience: *American Journal of Otolaryngology.* 25(5), pp. 301-307, 2004.
2. B.O. Ogundare, A. Bonnick and N. Bayley, Pattern of mandibular fractures in an urban major trauma center: *Journal of Oral & Maxillofacial Surgery.* 61(6), pp. 713-718, 2003.
3. C. Zahl, D. Muller, S. Felder and K.L. Gerlach, Cost of miniplate osteosynthesis for treatment of mandibular fractures: a prospective evaluation. *Gesundheitswesen,* 65(10): pp. 561-565, 2003.
4. W. Mollemans, F. Schutyser, N. Nadjmi and P. Suetens, Very fast soft tissue predictions with mass tensor model for maxillofacial surgery planning systems: *Proc. of 9th Annual Conference of the International Society for Computer Aided Surgery*, pp. 491 – 496, 2005.
5. E. Keeve, S. Girod and B. Girod, Craniofacial Surgery Simulation: *Proc. of Visualization in Biomedical Computing,* pp. 541 – 546, Springer 1996.
6. R. Enciso, A. Memon, U. Neumann, and J. Mah, The Virtual Cranio-Facial Patient Project: *Proc. of 3D Imaging*, (Medical Imaging Session) 2003.
7. A. Sarti, R. Gori, C. Marchetti, A. Bianchi and C. Lamberti, Maxillofacial Virtual Surgery from 3D CT Images: *VR in medicine*, Ed. by M. Akay and A. Marsh, IEEE EMBS Series, IEEE Press. 1999.
8. P.J. Besl and N.D. McKay, A Method for Registration of 3-D Shapes, *IEEE Trans. PAMI,* Vol. 14(2), pp. 239 – 256, 1992.
9. S. Granger, X. Pennec, and A. Roche, Rigid Point-Surface Registration Using an EM variant of ICP for Computer Guided Oral Implantology: *Proc. of the Int. Conf. on Medical Image Computing and Computer Assisted Intervention* (*MICCAI),* LNCS Vol. 2208, pp. 752-761, Utrecht, The Netherlands, 2001.
10. C.S. Chen, RANSAC-Based DARCES: A New Approach to Fast Automatic Registration of Partially Overlapping Range Images, *IEEE Trans. PAMI,* 21(11), pp. 1229 – 1234, 1999.
11. M. Rogers and J. Graham, Robust Active Shape Model Search for Medical Image Analysis, *Proc. of Int. Conf. on Medical Image Understanding and Analysis (MIUA),* Portsmouth, UK, 2002.
12. S.M. Bhandarkar, A.S. Chowdhury, Y. Tang, J. Yu and E.W. Tollner: Surface Matching Algorithms for Computer Aided Reconstructive Plastic Surgery: *Proc. of IEEE Int. Symposium on Biomedical Imaging (ISBI)*, pp. 740 - 743; Arlington, USA. 2004.
13. H. Goldstein, *Classical Mechanics*, Chapter 5, Addison-Wesley, 1982.
14. Y. Wang, B. Peterson and L. Staib, Shape-based 3D Surface Correspondence Using Geodesics and Local Geometry. *IEEE Conf. on Computer Vision and Pattern Recognition (CVPR),* Vol. II, pp. 644- 651, 2000.
15. K.M. Pohl, S.K. Warfield, R. Kikinis, W.E.L. Grimson and W.M. Wells, Coupling Statistical Segmentation and PCA Shape Modeling: *Proc. of the Int. Conf. on Medical Image Computing and Computer Assisted Intervention MICCAI,* Vol. I, pp. 151- 159, Saint-Marlo, France, 2004.

16. W.Y. Kim and A.C. Kak, 3-D Object Recognition Using Bipartite Matching Embedded in Discrete Relaxation, *IEEE Trans. PAMI,* 13(3), pp. 224 – 251, 1991.
17. H.W. Kuhn, The Hungarian method for the assignment problem, *Nav. Res. Log.* Quart. 2, 1955.
18. K.S. Arun, T.S. Huang and S.D. Blostein, Least-Squares Fitting of Two 3-D Point Sets, *IEEE Trans. PAMI,* Vol. 9(5), pp. 698 – 700, 1987.
19. S.M. Bhandarkar, A.S. Chowdhury, E.W. Tollner, J.C. Yu, E.W. Ritter and A. Konar: Surface Reconstruction for Computer Vision-based Craniofacial Surgery. *Proc. of IEEE Int. Workshop on Applications of Computer Vision (WACV)*, pp. 257 – 262, Breckenridge, USA. 2005.
20. S. Prima, S. Ourselin, and N. Ayache. Computation of the Mid-Sagittal Plane in 3D Brain Images. *IEEE Trans. on Medical Imaging*, 21(2), pp. 122-138, 2002.
21. B. Ardekani, J. Kershaw, M. Braun and I. Kanno, Automatic Detection of the Mid-Sagittal Plane in 3-D Brain Images, *IEEE Trans. Medical Imaging*, Vol. 16(6), 1997, 947- 952.
22. A. Tuzikov, O. Colliot and I. Bloch, Brain Symmetry plane computation in MR images using inertia axes and optimization, *Intl. Conf. on Pattern Recognition,* Vol. 1, pp. 10516-10519, 2002.
23. S. Gefan, Y. Fan, L. Bertrand and J. Nissanov, Symmetry-based 3D Brain Reconstruction, *IEEE Symp. Biomedical Imaging,* pp. 744 – 747, 2004.
24. L. Junck, J.G. Moen, G.D. Hutchins, M.B. Brown, and D.E. Kuhl, Correlation methods for the centering, rotation and alignment of functional brain images, *Journal of Nuclear Medicine.,* Vol. 31(7), pp. 1220- 1226, 1990.
25. I.H. Shames, *Mechanics of deformable solids*. Prentice-Hall Inc., Englewood Cliffs, NJ, 1964.
26. P.J. Besl, Surfaces in Early Range Image Understanding. *PhD Thesis,* Chapter 3*,* Univ. of Michigan. 1986.
27. M. Suk and S.M. Bhandarkar, *Three-dimensional Object Recognition from Range Images,* Chapter 7, Springer-Verlag, Tokyo. 1992.
28. *ImageJ* Website: http://rsb.info.nih.gov.
29. *3D Doctor* Website: http://www.ablesw.com/3d-doctor/3ddoctor.html.